Development of a kW Level-200 GHz Gyrotron FU CW GI with an Internal Quasi-optical Mode Convertor

**Yoshinori Tatematsu · Yuusuke Yamaguchi ·
Toshitaka Idehara · Takanori Ozeki · Ryosuke Ikeda ·
Tomohiro Kanemaki · Isamu Ogawa · Teruo Saito**

Abstract Development of gyrotrons with an internal mode convertor has started in Research Center for Development of Far-Infrared Region, University of Fukui (FIR FU). As the first gyrotron of such a kind, we have designed and manufactured Gyrotron FU CW GI. It operates at 203 GHz at fundamental cyclotron resonance. We have designed a cavity and a mode convertor under some constraints such as reuse of an electron gun and small diameter of a magnet bore. Designed output power is about 1 kW. We have succeeded in observation of a circular radiation pattern. The maximum observed output power is 0.5 kW for the setting cathode voltage of 20 kV and the beam current of 0.5 A. This success makes gyrotron development in FIR FU to proceed to a new stage.

1 Introduction

In FIR FU, a lot of high-frequency gyrotrons have been developed as sources in the millimeter and sub-millimeter wave range, which are applicable to various fields such as electron spin resonance (ESR), dynamic nuclear polarization (DNP)-nuclear magnetic resonance (NMR) spectroscopy and accurate measurements of hyperfine split of positronium [1–8]. The gyrotrons developed in FIR FU, FU series and FU CW series, are all linear type with axial output coupling, except Gyrotron FU CW I which was designed and constructed at IAP, RAS and Gycom [9]. In this type of gyrotron, the electromagnetic wave that oscillates in the cavity resonator transmits to the top window through the waveguide, maintaining the complex spatial structure of the field, and radiates through the window. Thus, the wave emitted from the window also has the complex structure and zero strength on the axis except for TE_{1n} mode oscillations. Such a beam is unsuitable as a power source for various applications. In order to improve this disadvantage, another type of gyrotron with radial output coupling is being developed. A quasi-optical mode convertor, which converts

Y. Tatematsu (✉) · Y. Yamaguchi · T. Idehara · T. Ozeki · R. Ikeda · T. Kanemaki · I. Ogawa · T. Saito
Research Center for Development of Far-Infrared Region, University of Fukui, Fukui 910-8507, Japan
e-mail: tatema@fir.u-fukui.ac.jp

the complex spatial structure of the field created in the cavity to a linearly polarized Gaussian beam, is built in the gyrotron [9–16]. In addition, this type of gyrotron has another advantage to separate the radiation from an electron beam and simplify the treatment of the radiation.

We have just started development of high-frequency gyrotrons of the latter type. Our first gyrotron with an internal quasi-optical mode convertor is called FU CW GI. The operation frequency is 203 GHz at fundamental cyclotron resonance which is applicable as a radiation source to measurements of the hyperfine split of positronium [4, 7] and pulsed ESR experiments. Since long time operation with kW output power is required in the positronium experiment, the target power is set as 1 kW with a cathode voltage 15 kV and a beam current 0.5 A. This gyrotron is a demountable type so that we can change components of the gyrotron such as the cavity, the mode convertor and the electron gun, and improve the design by considering the experimental results. Following Gyrotron FU CW GI, development plan of other gyrotrons, FU CW GII, FU CW GIII and FU CW CII, is now in progress. They are of sealed-off type.

The present main purpose is to confirm the validity of the design methods in Gyrotron FU CW GI development, such as power calculation, mode competition calculation and mode convertor design, before we start the manufacture of the following sealed-off tubes. We have some constraints in the design process, such as reuse of an electron gun and a small diameter of a room temperature bore of a magnet where the gyrotron is installed. The cavity dimension, the oscillation mode and the structure of the mode convertor have been optimized under such constraints. We also make confirmation of the operation properties of the gyrotron on measurement of the beam pattern radiated from the window.

2 Design consideration of gyrotron FU CW GI

To develop Gyrotron FU CW GI with a low cost, it was designed with some existing devices, which are an 8 T superconducting (SC) magnet and a triode-type electron gun. Furthermore, the fabrication was performed in the machine shop of University of Fukui. An initial drawing of the gyrotron is shown in Fig. 1. The magnetic field strength of the SC magnet can be increased up to 8 T. Three normal conducting gun coils are installed around the electron gun to control electron orbits emitted from it. Maximum current for these coils is 300 A, which generates 0.19 T at the center on the coil axis.

The quasi-optical mode convertor consists of a Vlasov launcher including a conventional helical cut waveguide and a quasi-parabolic mirror (mirror 1), and three mirrors (mirrors 2, 3 and 4). The waveguide launcher and two mirrors are installed at an axial position within the room temperature bore with 100 mm diameter of the SC magnet cryostat. Since a cooling water layer encircles the waveguide launcher and two mirrors, the dimension of the mirrors and the launcher radius are further limited. To make the beam width of radiation from the Vlasov launcher small, we should select TE_{mn} mode with a large m/χ_{mn}' as an oscillation mode, where χ_{mn}' is the n-th zero of the derivative of the m-th order Bessel function $J_m'(\chi)$. Thus, available oscillation modes are restricted. When the frequency of 203 GHz is fixed, the cavity radius R_c is determined by choosing an oscillation mode. If R_c is too small, its machine processing of production is difficult and a small alignment error in installation of the gyrotron on the magnet becomes serious. Thus, we set a condition that R_c is greater than 2.2 mm from our experience for the demountable gyrotrons. From the above investigation, we restricted the candidates of the oscillation mode to $TE_{m,2}$ with $4 < m < 10$.

The electron gun which was designed for another gyrotron is reused. The cathode radius is 14 mm. The value of the electron incident radius at the cavity R_b is closely related to the

**Fig. 1** Initial drawing of Gyrotron FU CW GI.
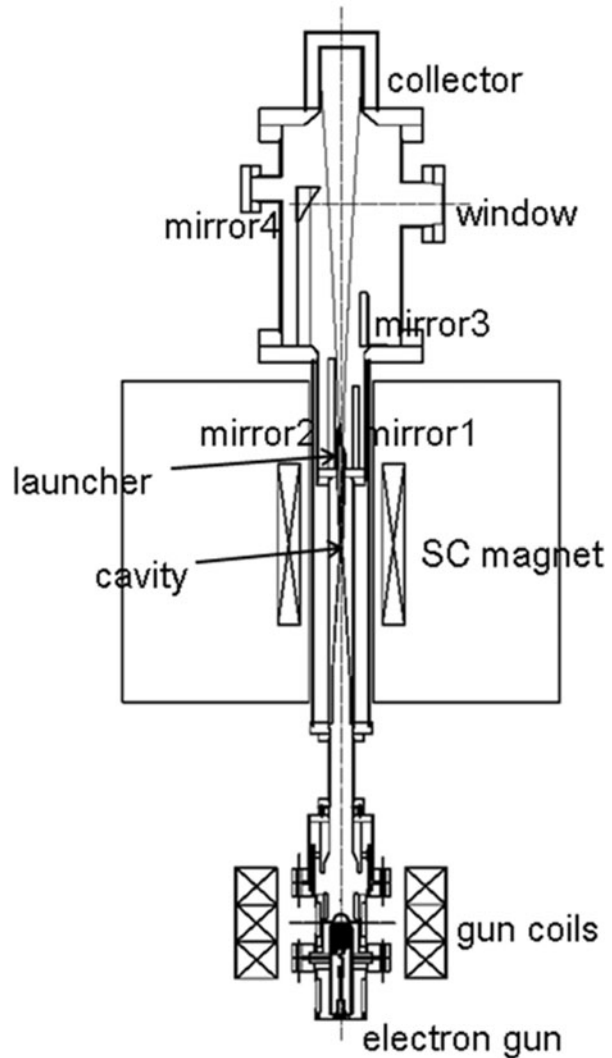
coupling between the electric field of the oscillation mode and electrons. The optimum R_b depends on the oscillation mode. Electron trajectories from the cathode into the cavity can be changed a little by changing an additional magnetic field generated by gun coils. The electrons can reach the cavity entrance with $1.2 < R_b < 2.2$ mm for the present electron gun. In Fig. 2, the coupling coefficients for some candidate modes are plotted against R_b, where, the cavity radius R_c was selected to match the frequency to 203 GHz for each mode. Since the optimum beam radius $R_{b,opt}$ exceeds 2.2 mm for higher modes with $m > 7$, they were excluded from the oscillation modes. The electron gun is to be located at a distance L_{gun} larger than 500 mm between the cathode and the cavity center (center of the SC magnet). When L_{gun} is 564 mm, $R_{b,opt}$'s giving the maximum coupling coefficient for co-rotating $TE_{5,2}$, $TE_{6,2}$ and $TE_{7,2}$ modes are obtained with the gun coil currents I_g of 21, 64 and 114 A, respectively. The value of $R_{b,opt}$ for counter rotating $TE_{5,2}$ mode is the same as that for co-$TE_{7,2}$ mode.

Fig. 2 Coupling coefficients of candidate modes.
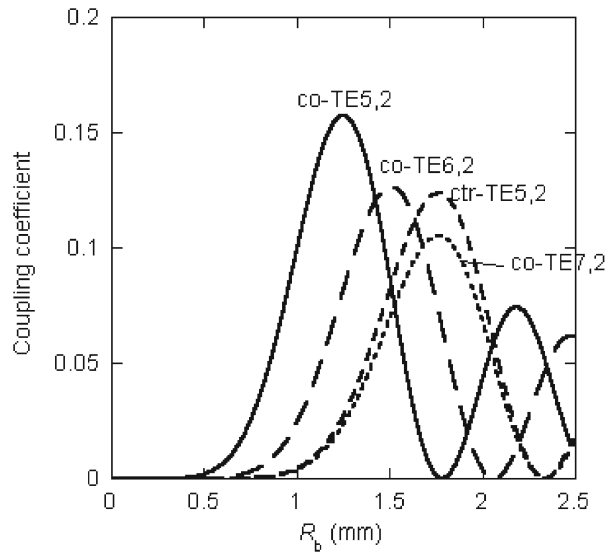
Under the assumption that the electron guiding center moves along a magnetic line of force and the adiabatic condition is satisfied, we can calculate the pitch factor α (the ratio of perpendicular velocity to parallel one) as a function of the anode–cathode voltage, $V_{a\text{-}k}$ [17]. Figure 3 shows the relation between α and $V_{a\text{-}k}$ for I_g=21, 64 and 114 A. The target value of α is set from 1.2 to 1.3 as shown by the light dark band in Fig. 3. For I_g=21 A, α rapidly changes for small variation of $V_{a\text{-}k}$, which will bring difficulty of the operation control. In addition, small value of $V_{a\text{-}k}$ results in a small electric field on the cathode surface. This is not suitable to reduce the space charge effect. From this point of view, counter-TE$_{5,2}$ and co-TE$_{7,2}$ modes are favorable.

Fig. 3 Relations between α and $V_{a\text{-}k}$.
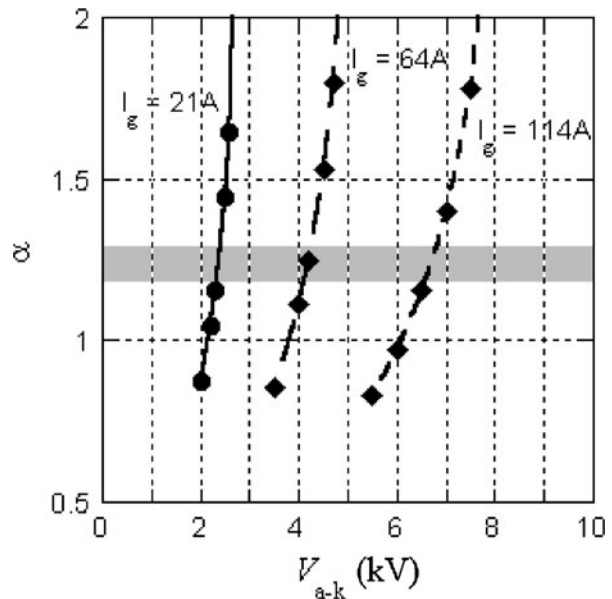
The axial position of the launcher has degrees of freedom. When it becomes higher, the risk for electrons to hit the launcher wall increases. For its lower position, the Brillouin angle θ_B should be smaller in order for the reflected radiation beam to come above the bore. In addition, the waveguide radius becomes larger to realize smaller θ_B and hence the dimension of the first mirror becomes relatively large. Moreover, the first mirror becomes a little large for its installation inside the bore if we adopt $TE_{7,2}$ mode. Therefore, we ruled out $TE_{7,2}$ mode, and $TE_{5,2}$ and $TE_{6,2}$ modes remained as the candidate.

Next we consider possibility of mode competition. Starting currents are plotted in Fig. 4. In calculations, the cathode voltage $V_k = 15$ kV and pitch factor $\alpha = 1.2$ were assumed. The values of R_c and R_b are 2.475, 1.25 mm in Fig. 4(a), 2.475, 1.77 mm in Fig. 4(b) and 2.76, 1.51 mm in Fig. 4(c), respectively. These values of R_c give the frequency of 203 GHz and those of R_b correspond to optimum values $R_{b,opt}$ for co-$TE_{5,2}$, counter-$TE_{5,2}$ and co-$TE_{6,2}$. Figure 4(c) indicates that $TE_{6,2}$ has a competing mode, $TE_{1,4}$. For this reason, we excluded $TE_{6,2}$ mode from the oscillation mode.

Next, oscillation power calculations including mode competition [18–20] were carried out. We solved a time-dependent equation for oscillation amplitudes. The axial field profile is self-consistently determined with interaction between RF field and the electron beam.
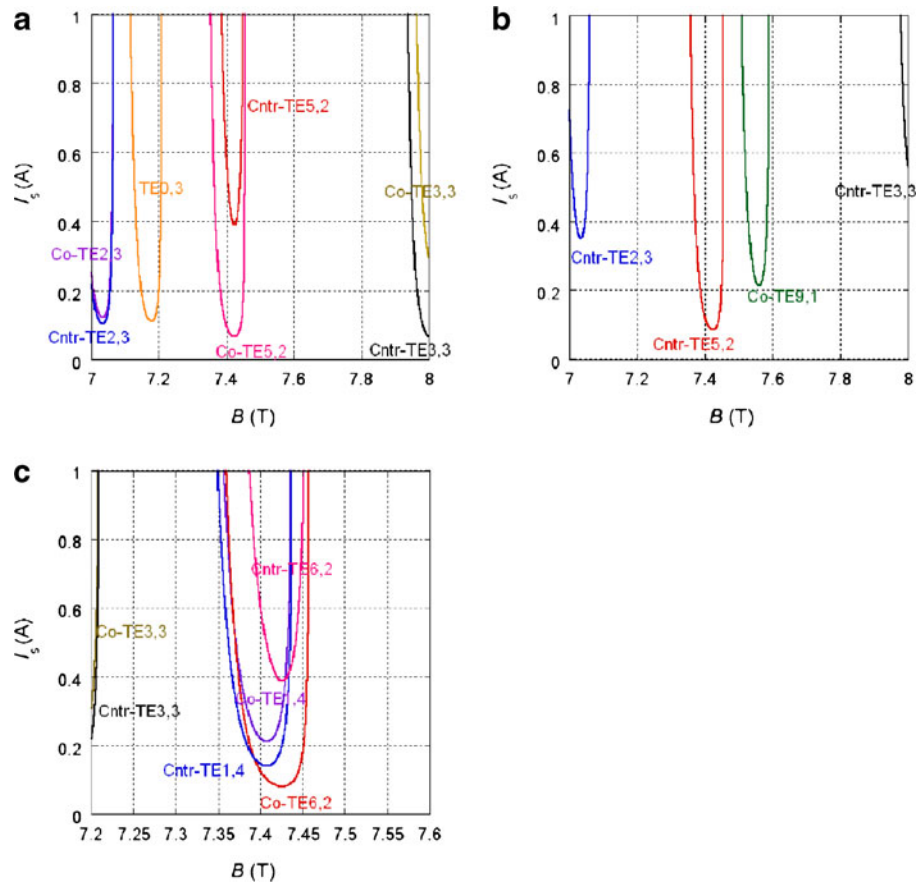

Fig. 4 Starting currents with optimized conditions for (a) co-$TE_{5,2}$, (b) ctr-$TE_{5,2}$, and (c) co-$TE_{6,2}$ modes.

Figure 5(a) and (b) show the calculated oscillation power P_{cav} at the cavity exit as functions of the cavity magnetic field strength B for the co-$TE_{5,2}$ and counter-$TE_{5,2}$ modes, respectively. The optimum incident radius $R_{b,opt}$ for each mode is substituted. Competing modes taken into calculations are co-$TE_{2,3}$, ctr-$TE_{2,3}$, ctr-$TE_{3,3}$ and $TE_{0,3}$ in Fig. 5(a) and ctr-$TE_{2,3}$, co-$TE_{9,1}$ and $TE_{0,3}$ in Fig. 5(b). In calculations, V_k =15 kV, the beam current I_b=0.5 A, and the pitch factor α=1.2 with no velocity spread were given. The thickness of the beam was not considered, either. The cavity length L_c=14 mm was assumed. In both cases, the only $TE_{5,2}$ mode oscillated and the others were not excited. The maximum value of P_{cav} of about 2 kW is expected for each case. We investigated R_b-dependence of P_{cav} at B=7.36 T, which is shown in Fig. 6. Large value of P_{cav} is maintained in a wide range of R_b for both rotational modes. The shallow hollow of P_{cav} seen around $R_{b,opt}$ for the co-$TE_{5,2}$ mode indicates that the assumed L_c is a little larger than the optimized one and energy reconversion from RF field to electrons occurs. On the other hand, for counter-$TE_{5,2}$ mode L_c=14 mm is the almost optimized length. From the power calculations, there is no reason to choose between co- and counter-rotating modes. Then, we have selected counter-$TE_{5,2}$ mode as the oscillation mode because of the controllability of α against changing of V_{a-k} as shown in Fig. 3. Thus, the direction of helical cut on the launcher is determined as left-hand rotating toward the top, which is counter to the direction of electron gyration motion, because the direction of the magnetic field is set upward in usual operations. However, if we reverse the direction of the magnetic field, the left-hand rotation of the helical cut becomes co-rotation to electron gyration motion, and we can also operate the co-$TE_{5,2}$ mode with the same launcher. We determined the dimension of the cavity as R_c=2.475 mm and L_c=14 mm. Corresponding diffractive quality factor Q_{dif} of the cavity is 3.2 x 10^3 and total quality factor Q_{tot} is 2.6 x 10^3. For B=7.36 T in Fig. 5(b), the power of 2.4 kW of the electron kinetic energy is transformed to the electromagnetic field power, 0.45 kW is lost on the cavity wall and the remaining 1.95 kW is extracted from the cavity.

Configuration of helical cut waveguide of the Vlasov launcher can be determined if its radius R_L and oscillation mode are given [21]. Then the quasi-parabolic mirror can be also determined, if the focal length L_f is given. We selected R_L=5.85 mm and L_f=17.55 mm. The second and the third mirrors usually have a role of phase correction to increase the conversion efficiency to a Gaussian beam. However, this time, they are simple plane mirrors for simplicity of manufacture. As shown below, plane mirrors are enough in the present case.
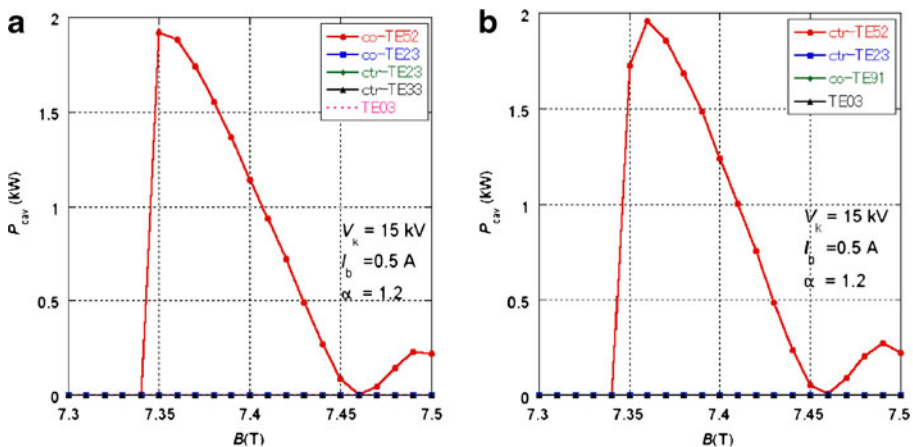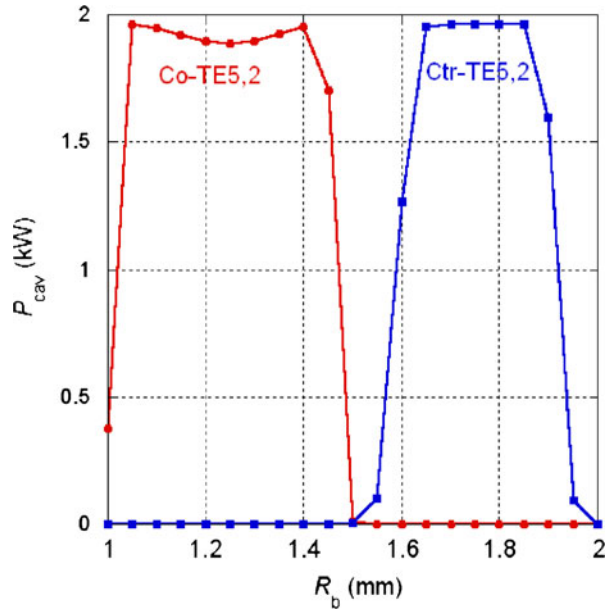

Fig. 5 Mode competition calculations with (a) R_b=1.25, (b) R_b=1.77 mm.

Fig. 6 Mode competition calcu-
lations between co- and
ctr-TE$_{5,2}$ modes at $B=7.36T$.

The two mirrors are placed in parallel each other. However, the center ray of the radiated
beam is not in a plane including launcher axis. Then, they are not placed perpendicular to the
direction of the center ray, but are slightly rotated around perpendicular axis for the center
ray to reach the center of the final mirror and to penetrate the window center. An ellipsoid
was adopted as the surface of the final mirror. Its shape was determined to make the cross
section of the reflection beam as circular as possible. Figure 7 shows an expected beam cross
section at 460 mm from the gyrotron window. The window is made of single crystal sapphire

Fig. 7 Radiation pattern calcula-
tion at the distance of 460 mm
from the window.
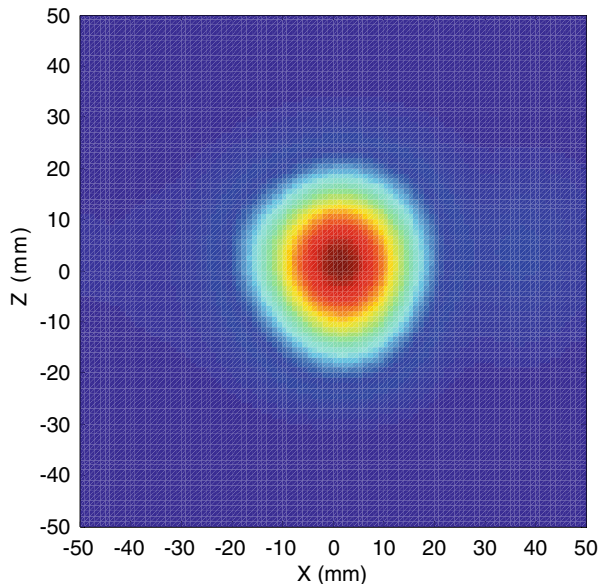
with the c-axis normal to the window surface. Its diameter is 60 mm and its thickness is 2.405 mm and the transmission rate of the electromagnetic wave at 203 GHz is higher than 95%.

The calculated oscillation power at the cavity exit was about 2 kW as shown in Fig. 5. By taking into consideration of a finite spread of R_b and α in the actual electron beam, a low conversion efficiency of around 70% to a Gaussian beam for the conventional Vlasov launcher, and the power loss at the window, it is expected that the reduced output power radiated from the window is about 1 kW.

All parts of Gyrotron FU CW GI except the electron gun and the vacuum window were manufactured in the machine shop in University of Fukui. Therefore, during the production phase, we could continue to change the gyrotron structure flexibly. As the result, some points have been improved from the initial drawing shown in Fig. 1. For example, we had changed the shape of the collector to decrease the electron beam density into it, by increasing its inner diameter at the entrance, tapering its wall and increasing its length. In the initial design, the final mirror position was not adjustable. However, it became movable for position adjustment by using a back port, where a bellows was attached. It can move radially by several mm and tilt by about 1 degree. The beam position on the window can shift at least vertically ±10 mm. and horizontally ±5 mm. Figure 8 shows a photograph of Gyrotron FU CW GI installed on the 8T-SC magnet. The output window is seen at the front side of the gyrotron. It has two pumping ports, top and bottom, as shown by two long flexible tubes in Fig. 8. A sufficiently good pressure lower than 10^{-5} Pa is kept with a turbo molecular pump.


Fig. 8 Photograph of gyrotron FU CW GI.

3 Experimental results

The solid line in Fig. 9 shows an example of time trace of oscillation signal measured with a pyro-electric detector placed in the front of the window. Here, the anode voltage V_a, measured from the ground voltage, was steadily applied and the cathode voltage V_k was periodically applied with the pulse width of 10 ms, during which the gyrotron oscillates. The setting values of the anode and cathode voltages on power supplies were −7 kV and −15 kV, respectively. The dashed line in Fig. 9 indicates the cathode voltage V_k and it was applied during $0<t<10$ ms. The value of the actual cathode voltage was about −14 kV, because of the voltage drop through a resistor inserted between the power supply and the cathode for protection to accidental large current. For $t>10$ ms, the power supply for V_k was turned off, however, V_k did not recovered to the ground voltage but was kept at the value of V_a (= −7 kV). The reason maybe as follows, a cathode is not shorted to the ground but is floating after $t=$ 10 ms. The cathode voltage was dropped till V_k became the same value of V_a because electrons are emitted from the cathode. After then, emission of electrons stops and V_k is kept at V_a. Then, V_k gradually increases to about −6 kV before the next pulse is turned on.

The radiation pattern of the power launched from the window was measured with an IR camera as the temperature increase on a vinyl chloride plate placed in the front of the window. The position of the final mirror was adjusted in order to make the center ray of the output beam to penetrate the center of the window. A result is shown in Fig. 10(a) and (b). A circular pattern was observed. Figure 10(b) is an expansion of the center region of Fig. 10(a). The length of one side is 60 mm. The distance of the plate from the gyrotron window is 115 mm. Here, the pulse width was 40 ms with repetition rate of 1 Hz. Horizontal and vertical temperature distributions are plotted in Fig. 10(c) and (d), respectively. They are well fitted by Gaussian curves. The origin in Fig. 10(c) and (d) are taken as the peak position of the fitting curves. The 1/e-radii of the fitting Gaussian profiles are 11 mm in horizontal and 10 mm in vertical. Thus, we have confirmed that the internal mode convertor works well.

Next, the dependence of oscillation strength on the magnetic field strength B was investigated. The signal intensity measured with the pyro-electric detector is plotted in Fig. 11. Here, The cathode voltage V_{k0} set at the power supply was −16 kV. The oscillation

Fig. 9 Time variations of the wave signal (solid line) and cathode voltage (dashed line).
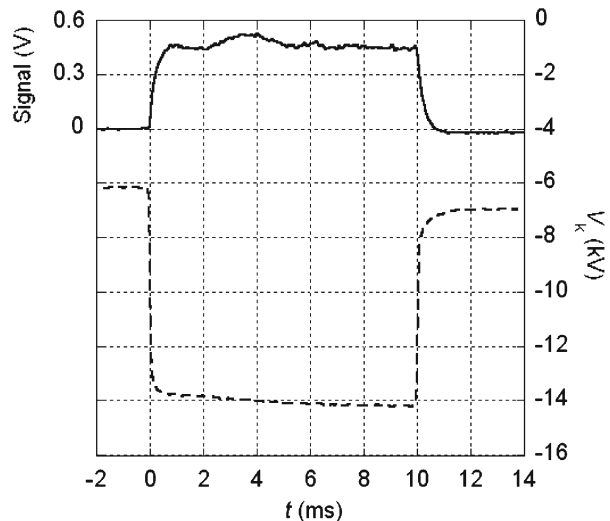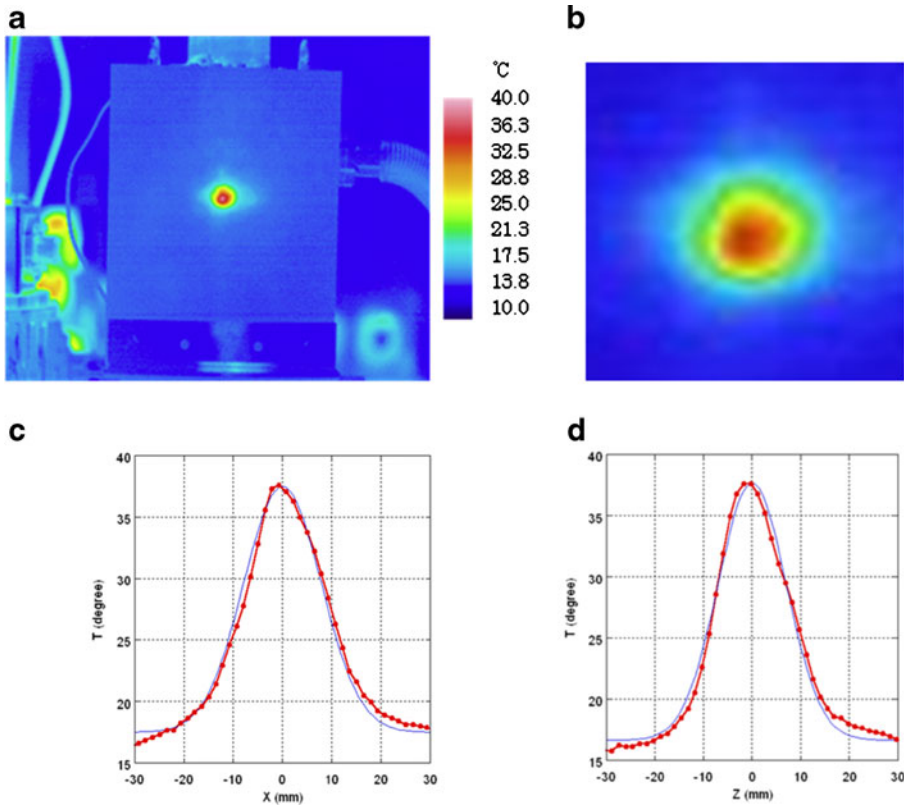
Fig. 10 (**a**) A measured radiation pattern with an IR camera. (**b**) Expansion of (**a**). The length of one side is 60 mm. (**c**) and (**d**) Temperature distributions (red thick lines) along the horizontal (**c**) and vertical (**d**) axes with Guassian fitting curves (blue thin lines).

signal was detected between 7.35T and 7.45T. This range well agrees with that expected from the calculation shown in Fig. 5. The magnetic field strength was precisely calibrated with ESR signal of DPPH. Thus, it is confirmed that the present radiated beam is converted from $TE_{5,2}$ mode oscillated in the cavity.

Figure 12 shows the result of measurement of the output power from the window as a function of the cathode voltage V_{k0} set at the power supply. It was measured with a water load just outside of the vacuum window. The voltage V_{k0} was changed and other parameters such as B, V_a and I_g were adjusted at the optimum values. The maximum output power obtained for each V_{k0} is plotted in Fig. 12. Beam current I_b was around 0.5 A. Maximum power of about 0.5 kW was obtained for $V_{k0}=20$ kV.

The oscillation frequency was measured with a heterodyne receiver system. The result is plotted in Fig. 13. The measured frequencies are a little smaller than the designed value of 203 GHz. The frequency almost linearly changes with B by about 0.3 GHz. The axial mode does not change within this range of B as seen from Fig. 11.

Moreover, longer pulse operation was tried and a 200 ms pulse width oscillation with repetition rate of 0.2 Hz has been successfully obtained with no deterioration in the vacuum condition. From this experimental result, it is suggested that the CW operation can be realized by the adoption of a DC power supply and a cooling system for the output window.

Fig. 11 Measured signal against B.
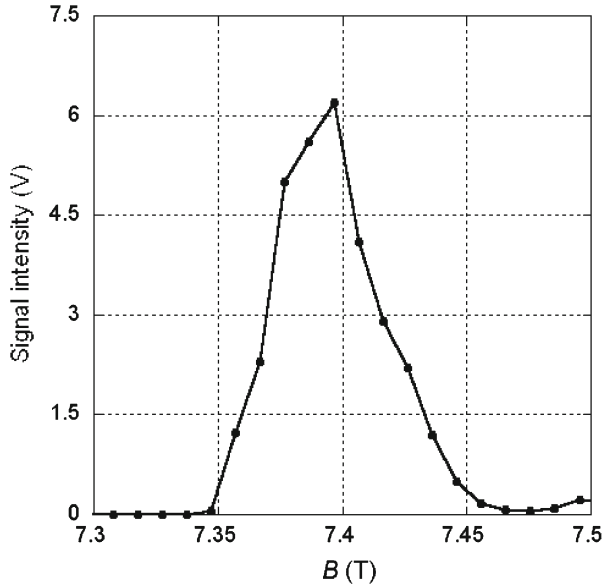
4 Discussion

We have obtained 0.5 kW as the maximum output power. However, the energy conversion efficiency was only 5%. We had expected to get around 1 kW output power. One of the reasons of this low power is the use of the existing electron gun. It was designed for a high power pulse gyrotron [22] operating with beam current $I_b > 10$ A, $V_k > 70$ kV and $V_{a-k} > 20$ kV. While, in the present operations, I_b, V_k and V_{a-k} are less than 1 A, 20 kV and 10 kV, respectively. The specification of the gun is too high for the present gyrotron. Width of the emission belt of the electron gun was determined for the large current operations and it is also too large for the present experiments. Therefore, beam quality of the electron beam is probably not good. The velocity

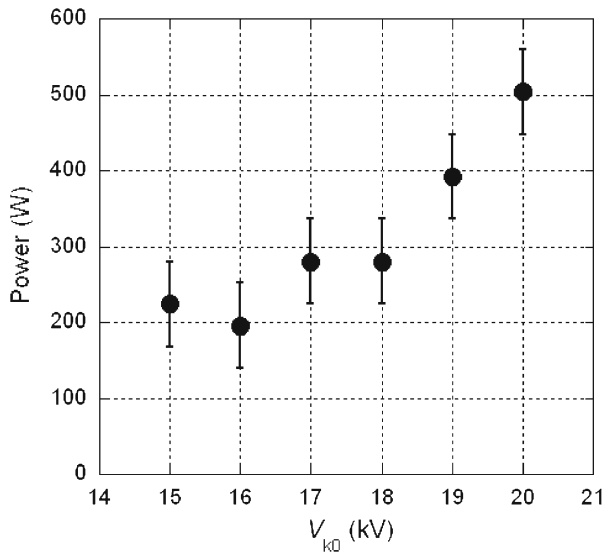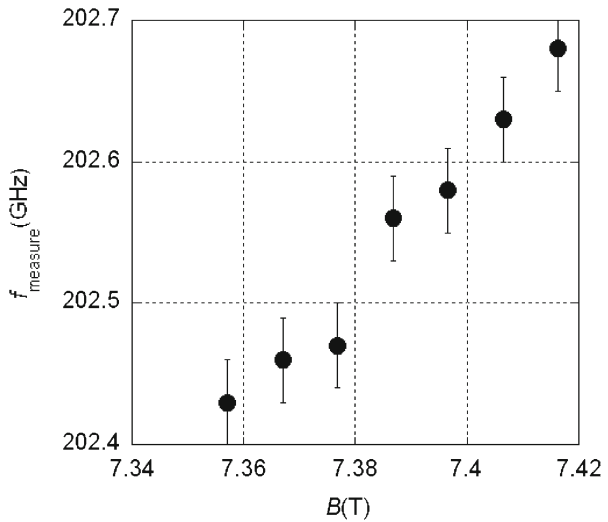**Fig. 12** Output power from the window measured with a water load.

Fig. 13 Measured frequency against B.

spreads $\delta v_\perp$ and $\delta v_{//}$ at the cavity entrance are estimated as 0.15 and 0.24, respectively with the EGUN code, where $\delta v_\perp = (v_{\perp max} - v_{\perp min})/v_{\perp average}$ and $\delta v_{//} = (v_{//max} - v_{//min})/v_{\perp average}$. If we had used an electron gun specially designed for Gyrotron FU CW GI, a much higher power would have been obtained. Fortunately, it is demountable, and then we can exchange it to the new one.

The observed frequency was a little lower than the designed value. It implies that the actual radius of the cavity is larger by several μm. The cavity should be also changed to tune the frequency just as we design. Improvement of Gyrotron FU CW GI is underway, in order to increase the output power up to 1 kW and to tune the frequency near 203 GHz for its application to measure the hyperfine structure of positronium.

We obtained the frequency change about 0.3 GHz. We didn't expect such a change because of the large Q value of the cavity. We have developed frequency continuous tunable gyrotrons such as Gyrotron FU CW IV [23], where oscillation frequency is changed continuously due to increase of the axial mode number of the electric field in the cavity and this behavior is explained as a gyro-backward oscillation (gyro-BWO) [24]. In the present case, however, we do not consider that the frequency change is due to excitation of higher axial modes. The frequency f with the axial mode number $l=2$ should be a little lower than the electron cyclotron frequency f_c for a gyro-BWO. However, the measured frequencies are still higher than f_c. In the range of the magnetic field strength in the frequency measurement is 7.34-7.42T, electromagnetic field with a single axial mode ($l=1$) oscillates, as indicated from the calculations in Fig. 5 (a) and (b). The second power peaks around 7.5T in Fig. 5(a) and (b) correspond to $l=2$ modes, although our calculation code cannot be applied to higher order axial modes in a rigorous manner. Thus, we cannot explain the frequency change as that in a gyro-BWO. The reason of the frequency change is not sure, but frequency variation is helpful in the experiment of positoronium hyperfine split. We hope that Gyrotron FU CW GI will be a suitable power source for this experiment after improvement.

5 Summary

We have developed Gyrotron FU CW GI with the internal mode convertor and have confirmed that it radiates a circular beam from the window. Operation test for the gyrotron

was carried out and 0.5 kW output power and frequencies from 202.4 to 202.7 GHz were observed. This gyrotron has a high potential to be a power source for the experiment on the analysis of hyperfine split of positoronium.

We have confirmed that our design method for the gyrotrons with an internal mode convertor is appropriate. It is the opening of FU CW G-series gyrotron development in FIR FU. The second gyrotron FU CW GII, oscillating at the frequency 394 GHz, second harmonic resonance with 0.1 kW output power, has been already developed as the radiation source for 600 MHz DNP-NMR spectroscopy. Moreover, the third gyrotron is being designed for construction in this fiscal year. It is an extension of Gyrotron FU CW GII and the frequency is the same as that of FU CW GII. It is also equipped with an internal mode convertor. A new electron gun will be specifically designed and a window cooling system will be added for completely continuous wave operation. It will be operated with the beam voltage in the range from 15 kV to 20 kV and the beam current lower than 0.6 A. The expected window power is 0.3 kW.

References

1. T. Idehara, K. Kosuga, La Agusu, I. Ogawa, H. Takahashi, M. E. Smith, R. Dupree, J. Infrared Milli. Terahz Waves **31**, 763 (2010).
2. T. Idehara, K. Kosuga, La Agusu, R. Ikeda, I. Ogawa, T. Saito, Y. Matsuki, K. Ueda, T. Fujiwara, J. Infrared Milli. Terahz Waves **31**, 775 (2010).
3. T. Idehara, I. Ogawa, S. Mitsudo, Y. Tatematsu, T. Saito, in "Proceedings of 3rd International Workshop on Far Infrared Technologies 2010" (2010) 3.
4. S. Asai, T. Suehara, T.Yamazaki, G. Akimoto, A. Miyazaki, T. Namba, T. Kobayashi, H. Saito, T. Idehara, I. Ogawa, Y. Urushizaki, S. Sabchevski, in "Proceedings of 3rd International Workshop on Far Infrared Technologies 2010" (2010) 77.
5. A. Miyazaki, T. Yamazaki, T. Suehara, T. Namba, S. Asai, T. Kobayashi, H. Saito, T. Idehara, I. Ogawa, Y. Urushizaki and S. Sabchevski, Material Sceince Forum **666**, 133 (2011).
6. T. Fujiwara, Y. Matsuki, H. Takahashi, K. Ueda, T. Idehara, I. Ogawa, M. Toda, in "Proceedings of 3rd International Workshop on Far Infrared Technologies 2010" (2010) 150.
7. T. Suehara, A. Miyazaki, T. Yamazaki, G. Akimoto, A. Ishida, T. Namba, S. Asai, T. Kobayashi, H. Saito, M. Yoshida, T. Idehara, I. Ogawa, Y. Urushizaki, S. Sabchevski, in "Proceedings of 3rd International Workshop on Far Infrared Technologies 2010" (2010) 199.
8. R. Ikeda, T. Idehara, I. Ogawa, K. Kosuga, T. Saito, Y. Matsuki, K. Ueda, T. Fujiwara, T. H. Chang, in "Proceedings of 3rd International Workshop on Far Infrared Technologies 2010" (2010) 206.
9. V. E. Zapevalov, V. K. Lygin, O. V. Malygin, M. A. Moiseev, V. I. Khizhnyak, V. P. Karpov, E. M. Tai, T. Idehara, S. Mitsudo, I. Ogawa, T. Saito, Radiophys. Quantum Electronics **50**, 420 (2007).
10. G. G. Denisov, A. N. Kuftin, V. I. Malygin, N. P. Venedictov. D. V. Vinogradov, V. E. Zapevalov, Int. J. Electrronics **72**, 1079 (1992).
11. K. Sakamoto, M. Tsuneoka, A. Kasugai, T. Imai, T. Kariya, K. Hayashi, Y. Mitsunaka, Phys. Rev. Lett. **26**, 3532 (1994).
12. M. Thumm, in "Generation and Application of High Power Microwaves" ed. R. A. Cairns and A. D. R. Phelps (A NATO Advanced Study Institute, The Scottish Universities Summer School in Physics, 1997).
13. M. K. Hornstein, V. S. Bajaj, R. G. Griffin, R. J. Temkin, IEEE Trans. Plasma Science **34**, 524 (2006).
14. T. Saito, T. Nakano, H. Hoshizuki, K. Sakai , Y. Tatematsu, S. Mitsudo, I. Ogawa, T. Idehara . V. E. Zapevalov, Int J. Infrared Milli. Waves **28**, 1063 (2007).
15. V. S. Bajaj, M. K. Hornstein, K. E. Kreischer, J. R. Sirigiri, P. P. Woskov, M. L. Mak-Jurkauskas, J. Herzfeld, R. J. Temkin, R. G. Griffin, J. Magnetic Resonance **189**, 251 (2007).
16. A. C. Torrezan, S.T. Han, I. Mastovsky, M. A. Shapiro, J. R. Sirigiri, R. J. Temkin, A. B. Barnes, and R. G. Griffin, IEEE Trans. Plasma Science **38**, 1150 (2010).

17. B. Piosczuk, Chap. 5 in "Gyrotron Oscillation, Their Principles and Practice", ed. by C. J. Edgcombe (Taylor & Francis, 1993).
18. N. A. Zavolsky, G. S. Nusinovich, and A. B. Pavelyev, in Gyrotrons, ed. by A.V. Gaponov-Grekhov (IAP, ASR, Gorky, 1989),.
19. L. Agusu, T. Idehara, H. Mori, T. Saito, I. Ogawa, S. Mitsudo, Int J Infrared Milli Waves 28, 315 (2007).
20. O. Dumbrajs, T. Idehara, Int. J. Infrared Milli. Waves 29, 232 (2008).
21. A. Möbius and M. Thumm, Chap. 7 in "Gyrotron Oscillation, Their Principles and Practice", ed. C. J. Edgcombe (Taylor & Francis, 1993).
22. V. N. Manuilov, T. Idehara, T. Saito, L. Agusu, T. Hayashi, I. Ogawa, Int. J. Infrared Milli. Waves 29, 1103 (2008).
23. T. Idehara, I. Ogawa, La Agusu, T. Kanemaki, S. Mitsudo, T. Saito, T. Fujiwara and H. Takahashi, Int J Infrared Milli Waves 28, 433 (2007).
24. T. H. Chang, T. Idehara, I. Ogawa, L. Agusu, and S. Kobayashi, J. Appl. Phys. 105, 063304 (2009).